

A new Meshless Local Petrov-Galerkin (MLPG) approach in computational mechanics

S. N. Atluri, T. Zhu

Abstract A local symmetric weak form (LSWF) for linear potential problems is developed, and a truly meshless method, based on the LSWF and the moving least squares approximation, is presented for solving potential problems with high accuracy. The essential boundary conditions in the present formulation are imposed by a penalty method. The present method does not need a “finite element mesh”, either for purposes of interpolation of the solution variables, or for the integration of the “energy”. All integrals can be easily evaluated over regularly shaped domains (in general, spheres in three-dimensional problems) and their boundaries. No post-smoothing technique is required for computing the derivatives of the unknown variable, since the original solution, using the moving least squares approximation, is already smooth enough. Several numerical examples are presented in the paper. In the example problems dealing with Laplace & Poisson’s equations, high rates of convergence with mesh refinement for the Sobolev norms $\|\cdot\|_0$ and $\|\cdot\|_1$ have been found, and the values of the unknown variable and its derivatives are quite accurate. In essence, the present meshless method based on the LSWF is found to be a simple, efficient, and attractive method with a great potential in engineering applications.

1 Introduction

The Galerkin finite element method, due to its profound roots in generalized variational principles and its ease of use, has found extensive engineering acceptance as well as a commercial market. Compared with its convenience and flexibility in use, the finite element method has been plagued for a long time by the inherent problems such as

locking, poor derivative solutions, etc. In contrast, although only a boundary discretization is necessary for linear boundary value problems, the boundary element method is constrained to the cases where the infinite space fundamental solution for (at least the highest linear) differential operator of the problem must be available. Besides, in the BEM, the evaluation of the unknown function and/or its gradients at any single point within the domain of the problem involves the calculation of an integral over the entire global boundary, which is tedious and inefficient. In solving the nonlinear problems, both FEM and BEM inevitably have to deal with the nonlinear terms in the domain of the problem.

An attractive option for such problems is the meshless discretization or a finite point discretization approach, which has been popularized in recent years. Several meshless methods have been reported in literature, such as the diffuse element method (Nayroles et al., 1992), the element free Galerkin method (Belytschko et al., 1994; Organ et al., 1996; Zhu and Atluri, 1998), the reproducing kernel particle method (Liu et al., 1996). These methods need shadow elements to evaluate the domain integrals (corresponding to the “energy”) over the entire domain of the problem, and so far, have been applied mainly to solve linear problems. Another meshless method, for solving linear and nonlinear problems, based on the local boundary integral equation was proposed in Zhu, Zhang and Atluri (1998a, b). This method requires no domain and boundary elements (either for interpolation purposes, or for evaluation of the integrals) to implement the formulation, and is very efficient in solving linear and nonlinear problems. However, singular integrals appear in the local boundary integral equation (defined only over a sphere centered at each point in question), to which special attention should be paid.

In the present work, a local symmetric weak form (LSWF) is developed. A true meshless formulation based on the presently developed local symmetric weak form is proposed to solve linear potential problems. The essential boundary conditions in the present formulation are imposed by a penalty method. This method does not need elements or meshes, either for interpolation purposes, or for integration (of “energy”) purposes. All integrals are carried out only on spheres (in 3-D or circles in 2-D) centered at each point in question. The present method is also more flexible and easier in dealing with nonlinear problems than the conventional FEM, EFG and BEM. Although mainly 2-D problems described by a harmonic operator are considered in the present paper for

Communicated by G. Yagawa, 12 January 1998

S. N. Atluri, T. Zhu
Center for Aerospace Research & Education,
7704 Boelter Hall, University of California at Los Angeles,
Los Angeles, CA 90095-1600, USA

Correspondence to: S. N. Atluri

This work was supported by research grants from the Office of Naval Research, and the Federal Aviation Administration, with Y. D. S. Rajapakse, and C. C. Seher as cognizant program officials.

illustrative purposes only, the method can be easily applied to elasticity as well as other multi-dimensional linear and nonlinear boundary value problems.

In the present paper, by “the support of node \mathbf{x}_i ” we mean a sub-domain (usually taken as a circle of radius r_i) in which the weight function w_i in the MLS approximation, associated with node \mathbf{x}_i , is non-zero; by “the domain of definition” of an MLS approximation for the trial function at any point \mathbf{x} (hereinafter simply called as the “domain of definition of point \mathbf{x} ”) we mean a sub-domain which covers all the nodes whose weight functions do not vanish at \mathbf{x} ; by “the domain of influence of node \mathbf{x}_i ” we denote a sub-domain in which all the nodes have non-zero couplings with the nodal values at \mathbf{x}_i , in the system stiffness matrix; and by the “symmetric weak form” we mean the weighted residual form for the differential equation, which is integrated by parts enough times such that the differentiability requirements for the trial and test functions are the same. In our implementation, the domain of influence of a node is the union of the domains of definition of all points (in general, but the integration-quadrature points in specific) in the local domain of the source point (node). We do not intend to mean these to be versatile definitions, but rather, explanations of our terminology.

The following discussion begins with the brief description of the moving least squares (MLS) approximation in Sect. 2. The local symmetric weak form and its numerical implementation are developed in Sect. 3 and 4, respectively. Numerical examples for 2-D potential problems are given in Sect. 5. The paper ends with conclusions and discussions in Sect. 6.

2

The MLS approximation scheme

In general, a meshless method, which is required to preserve the local character of the numerical implementation, uses a local interpolation or approximation to represent the trial function with the values (or the fictitious values) of the unknown variable at some randomly located nodes. A variety of local interpolation schemes that interpolate the data at randomly scattered points in two or more independent variables is available.

In order to make the current formulation fully general, it needs a relatively direct local interpolation or approximation scheme with reasonably high accuracy and with ease of extension to n -dimensional problems. The moving least squares (MLS) approximation may be considered as one of such schemes, and is used in the current work.

Consider a sub-domain $\Omega_{\mathbf{x}}$, the neighborhood of a point \mathbf{x} and denoted as the domain of definition of the MLS approximation for the trial function at \mathbf{x} , which is located in the problem domain Ω . To approximate the distribution of function u in $\Omega_{\mathbf{x}}$, over a number of randomly located nodes $\{\mathbf{x}_i\}$, $i = 1, 2, \dots, n$, the Moving Least Squares approximant $u^h(\mathbf{x})$ of u , $\forall \mathbf{x} \in \Omega_{\mathbf{x}}$, can be defined by

$$u^h(\mathbf{x}) = \mathbf{p}^T(\mathbf{x})\mathbf{a}(\mathbf{x}) \quad \forall \mathbf{x} \in \Omega_{\mathbf{x}} \quad (1)$$

where $\mathbf{p}^T(\mathbf{x}) = [p_1(\mathbf{x}), p_2(\mathbf{x}), \dots, p_m(\mathbf{x})]$ is a complete monomial basis of order m ; and $\mathbf{a}(\mathbf{x})$ is a vector containing coefficients $a_j(\mathbf{x})$, $j = 1, 2, \dots, m$ which are functions of the

space coordinates $\mathbf{x} = [x^1, x^2, x^3]^T$. For example, for a 2-D problem,

$$\mathbf{p}^T(\mathbf{x}) = [1, x^1, x^2], \quad \text{linear basis; } m = 3; \quad (2a)$$

$$\mathbf{p}^T(\mathbf{x}) = [1, x^1, x^2, (x^1)^2, x^1x^2, (x^2)^2], \quad \text{quadratic basis; } m = 6, \quad (2b)$$

and for a 3-D problem

$$\mathbf{p}^T(\mathbf{x}) = [1, x^1, x^2, x^3], \quad \text{linear basis; } m = 4; \quad (3a)$$

$$\mathbf{p}^T(\mathbf{x}) = [1, x^1, x^2, x^3, (x^1)^2, (x^2)^2, (x^3)^2, x^1x^2, x^2x^3, x^1x^3] \quad \text{quadratic basis; } m = 10. \quad (3b)$$

The coefficient vector $\mathbf{a}(\mathbf{x})$ is determined by minimizing a weighted discrete L_2 norm, defined as:

$$J(\mathbf{x}) = \sum_{i=1}^n w_i(\mathbf{x}) [\mathbf{p}^T(\mathbf{x}_i)\mathbf{a}(\mathbf{x}) - \hat{u}_i]^2 \quad (4)$$

$$= [\mathbf{P} \cdot \mathbf{a}(\mathbf{x}) - \hat{\mathbf{u}}]^T \cdot \mathbf{W} \cdot [\mathbf{P} \cdot \mathbf{a}(\mathbf{x}) - \hat{\mathbf{u}}],$$

where $w_i(\mathbf{x})$ is the weight function associated with the node i , with $w_i(\mathbf{x}) > 0$ for all \mathbf{x} in the support of $w_i(\mathbf{x})$, \mathbf{x}_i denotes the value of \mathbf{x} at node i , n is the number of nodes in $\Omega_{\mathbf{x}}$ for which the weight functions $w_i(\mathbf{x}) > 0$, the matrices \mathbf{P} and \mathbf{W} are defined as

$$\mathbf{P} = \begin{bmatrix} \mathbf{p}^T(\mathbf{x}_1) \\ \mathbf{p}^T(\mathbf{x}_2) \\ \dots \\ \mathbf{p}^T(\mathbf{x}_n) \end{bmatrix}_{n \times m}, \quad (5)$$

$$\mathbf{W} = \begin{bmatrix} w_1(\mathbf{x}) & \dots & \mathbf{0} \\ \dots & \dots & \dots \\ \mathbf{0} & \dots & w_n(\mathbf{x}) \end{bmatrix}, \quad (6)$$

and

$$\hat{\mathbf{u}}^T = [\hat{u}_1, \hat{u}_2, \dots, \hat{u}_n]. \quad (7)$$

Here it should be noted that \hat{u}_i , $i = 1, 2, \dots, n$ in Eqs. (4) and (7) are the fictitious nodal values, and not the nodal values of the unknown trial function $u^h(\mathbf{x})$ in general (See Fig. 1 for a simple one dimensional case for the distinction between u_i and \hat{u}_i .)

The stationarity of J in Eq. (4) with respect to $\mathbf{a}(\mathbf{x})$ leads to the following linear relation between $\mathbf{a}(\mathbf{x})$ and $\hat{\mathbf{u}}$.

$$\mathbf{A}(\mathbf{x})\mathbf{a}(\mathbf{x}) = \mathbf{B}(\mathbf{x})\hat{\mathbf{u}} \quad (8)$$

where the matrices $\mathbf{A}(\mathbf{x})$ and $\mathbf{B}(\mathbf{x})$ are defined by

$$\mathbf{A}(\mathbf{x}) = \mathbf{P}^T \mathbf{W} \mathbf{P} = \mathbf{B}(\mathbf{x}) \mathbf{P} = \sum_{i=1}^n w_i(\mathbf{x}) \mathbf{p}(\mathbf{x}_i) \mathbf{p}^T(\mathbf{x}_i), \quad (9)$$

$$\mathbf{B}(\mathbf{x}) = \mathbf{P}^T \mathbf{W} = [w_1(\mathbf{x}) \mathbf{p}(\mathbf{x}_1), w_2(\mathbf{x}) \mathbf{p}(\mathbf{x}_2), \dots, w_n(\mathbf{x}) \mathbf{p}(\mathbf{x}_n)]. \quad (10)$$

The MLS approximation is well defined only when the matrix \mathbf{A} in Eq. (8) is non-singular. It can be seen that this is the case if and only if the rank of \mathbf{P} equals m . A necessary condition for a well-defined MLS approximation is that at least m weight functions are non-zero (i.e. $n \geq m$) for each sample point $\mathbf{x} \in \Omega$ and that the nodes in $\Omega_{\mathbf{x}}$ will

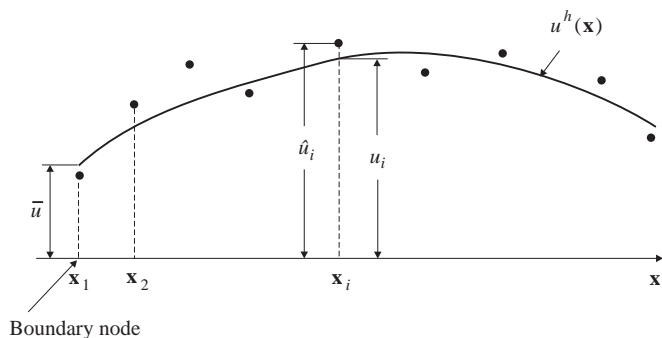


Fig. 1. The distinction between u_i and \hat{u}_i

not be arranged in a special pattern such as on a straight line. Here a sample point may be a nodal point under consideration or a quadrature point.

Solving for $\mathbf{a}(\mathbf{x})$ from Eq. (8) and substituting it into Eq. (1) gives a relation which may be written as the form of an interpolation function similar to that used in FEM, as

$$u^h(\mathbf{x}) = \Phi^T(\mathbf{x}) \cdot \hat{\mathbf{u}} = \sum_{i=1}^n \phi_i(\mathbf{x}) \hat{u}_i; \quad u^h(\mathbf{x}_i) \equiv u_i \neq \hat{u}_i; \quad \mathbf{x} \in \Omega_x \quad (11)$$

where

$$\Phi^T(\mathbf{x}) = \mathbf{p}^T(\mathbf{x}) \mathbf{A}^{-1}(\mathbf{x}) \mathbf{B}(\mathbf{x}) \quad (12)$$

or

$$\phi_i(\mathbf{x}) = \sum_{j=1}^m p_j(\mathbf{x}) [\mathbf{A}^{-1}(\mathbf{x}) \mathbf{B}(\mathbf{x})]_{ji} . \quad (13)$$

$\phi_i(\mathbf{x})$ is usually called the shape function of the MLS approximation corresponding to nodal point \mathbf{y}_i . From Eqs. (10) and (13), it may be seen that $\phi_i(\mathbf{x}) = 0$ when $w_i(\mathbf{x}) = 0$. In practical applications, $w_i(\mathbf{x})$ is generally

chosen such that it is non-zero over the support of nodal points \mathbf{y}_i (see Fig. 2). The support of the nodal point \mathbf{y}_i is usually taken to be a circle of radius r_i , centered at \mathbf{y}_i . The fact that $\phi_i(\mathbf{x}) = 0$, for \mathbf{x} not in the support of nodal point \mathbf{y}_i preserves the local character of the Moving Least Squares approximation.

The smoothness of the shape functions $\phi_i(\mathbf{x})$ is determined by that of the basis functions and of the weight functions. Let $C^k(\Omega)$ be the space of k -th continuously differentiable functions. If $w_i(\mathbf{x}) \in C^k(\Omega)$ and $p_j(\mathbf{x}) \in C^l(\Omega)$, $i = 1, 2, \dots, n$; $j = 1, 2, \dots, m$, then $\phi_i(\mathbf{x}) \in C^r(\Omega)$ with $r = \min(k, l)$.

The partial derivatives of $\phi_i(\mathbf{x})$ are obtained as (Beltychko et al., 1994)

$$\phi_{i,k} = \sum_{j=1}^m [p_{j,k}(\mathbf{A}^{-1} \mathbf{B})_{ji} + p_j(\mathbf{A}^{-1} \mathbf{B}_{,k} + \mathbf{A}_{,k}^{-1} \mathbf{B})_{ji}] \quad (14)$$

in which $\mathbf{A}_{,k}^{-1} = (\mathbf{A}^{-1})_{,k}$ represents the derivative of the inverse of \mathbf{A} with respect to x^k , which is given by

$$\mathbf{A}_{,k}^{-1} = -\mathbf{A}^{-1} \mathbf{A}_{,k} \mathbf{A}^{-1} \quad (15)$$

where, $(\)_{,i}$ denotes $\partial(\) / \partial x^i$.

In implementing the MLS approximation for the present local symmetric weak form, the basis functions and weight functions should be chosen at first. Both Gaussian and spline weight functions with compact supports can be considered in the present work. The Gaussian weight function corresponding to node i may be written as

$$w_i(\mathbf{x}) = \begin{cases} \frac{\exp[-(d_i/c_i)^{2k}] - \exp[-(r_i/c_i)^{2k}]}{1 - \exp[-(r_i/c_i)^{2k}]} & 0 \leq d_i \leq r_i \\ 0 & d_i \geq r_i \end{cases} \quad (16)$$

where $d_i = |\mathbf{x} - \mathbf{x}_i|$ is the distance from node \mathbf{x}_i to point \mathbf{x} ; c_i is a constant controlling the shape of the weight function w_i and therefore the relative weights; and r_i is the size of the support for the weight function w_i and determines the support of node \mathbf{x}_i . In the present computation,

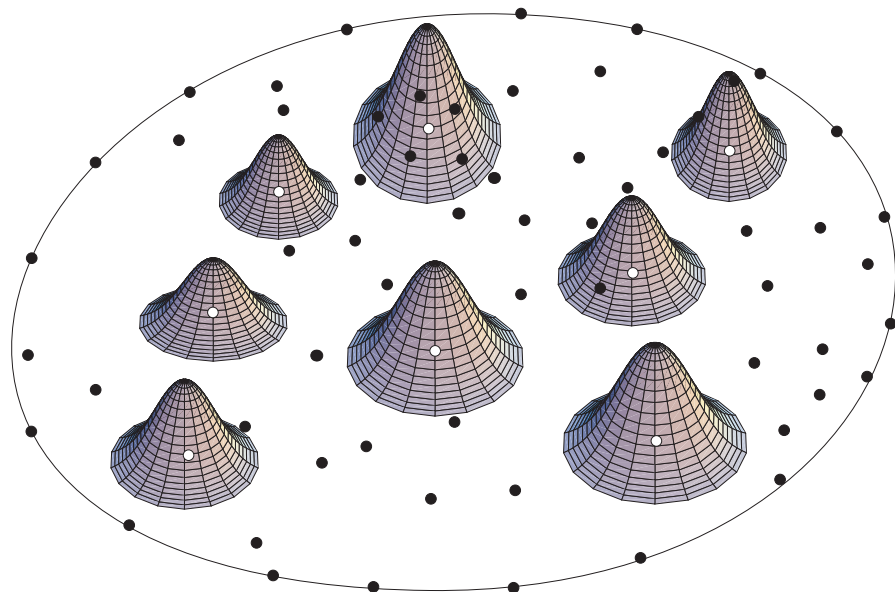


Fig. 2. The shapes of weight functions $w_i(\mathbf{x})$

$k = 1$ was chosen. It can be easily seen that the Gaussian weight function is C^0 continuous over the entire domain Ω . Therefore, the shape functions and the trial function are also C^0 continuous over the entire domain. Even though the definition of all constants c_i is more or less arbitrary, they do effect the computational results significantly. Lu, Belytschko and Gu (1994) recommended a method to chose constants c_i , however, better methods to chose these constants should be explored.

A spline weight function is defined as

$$w_i(\mathbf{x}) = \begin{cases} 1 - 6\left(\frac{d_i}{r_i}\right)^2 + 8\left(\frac{d_i}{r_i}\right)^3 - 3\left(\frac{d_i}{r_i}\right)^4 & 0 \leq d_i \leq r_i \\ 0 & d_i \geq r_i \end{cases} \quad (17)$$

It can also be easily seen that the spline weight function (17) is C^1 continuous over the entire domain Ω . Therefore, the shape functions and the trial function are also C^1 continuous over the entire domain.

Here, distinction between “the domain of definition of an MLS approximation for the trial function at a point” (herein after simplified as “the domain of definition of a point”) and the support of a node should be noted. The domain of definition of a point \mathbf{x} is a domain in which $w_i(\mathbf{x}) \neq 0, i = 1, 2, \dots, n$ and the support of node j is a circle (sphere) of radius r_j , centered at \mathbf{x}_j , in which $w_j \neq 0$ (see Fig. 3 and Mukherjee and Mukherjee 1997).

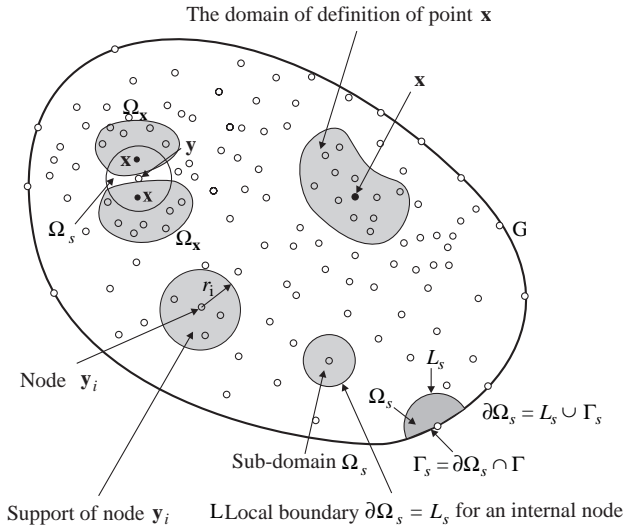


Fig. 3. The local domains, the supports of nodes, the domain of definition of the MLS approximation for the trial function at a point, and the domain of influence of a source point (node): (1) The domain of definition of the MLS approximation, Ω_x , for the trial function at any point \mathbf{x} is the domain over which the MLS is defined, i.e., Ω_x covers all the nodes whose weight functions do not vanish at \mathbf{x} . (2) The domain of influence for source point \mathbf{y} is the union of all $\Omega_x, \forall \mathbf{x} \in \Omega_s$ (taken to be a circular domain of radius r_0 in this paper). (3) The support of source point \mathbf{y}_i is a sub-domain (taken to be a circle of radius r_i for convenience) in which the weight function w_i corresponding to this node is non-zero. Note that the “support” of \mathbf{y}_i is distinct and different from the “domain” of influence of \mathbf{y}_i

It is easy for the moving least squares approximation to attain higher order of continuity for the shape functions and the trial function by constructing a more continuous weight function. A simple way is to use higher order spline functions.

The size of support, r_i , of the weight function w_i associated with node i should be chosen such that r_i should be large enough to have sufficient number of nodes covered in the domain of definition of every sample point ($n \geq m$) to ensure the regularity of \mathbf{A} . A very small r_i may result in a relatively large numerical error in using Gauss numerical quadrature to calculate the entries in the system matrix. On the other hand, r_i should also be small enough to maintain the local character of the MLS approximation.

3 Local symmetric weak form (LSWF)

Although the present approach is fully general in solving general boundary value problems, only the linear Poisson’s equation is used in the following, to demonstrate the formulation. The Poisson’s equation can be written as

$$\nabla^2 u(\mathbf{x}) = p(\mathbf{x}) \quad \mathbf{x} \in \Omega \quad (18)$$

where $p(\mathbf{x})$ is a given source function, and the domain Ω is enclosed by $\Gamma = \Gamma_u \cup \Gamma_q$, with boundary conditions

$$u = \bar{u} \quad \text{on} \quad \Gamma_u, \quad (19a)$$

$$\frac{\partial u}{\partial n} \equiv q = \bar{q} \quad \text{on} \quad \Gamma_q \quad (19b)$$

where \bar{u} and \bar{q} are the prescribed potential and normal flux, respectively, on the essential boundary Γ_u and on the flux boundary Γ_q , and n is the outward normal direction to the boundary Γ .

In the Galerkin finite element, and element free Galerkin methods, which are based on the global Galerkin formulation, one uses the global weak form over the entire domain Ω to solve the problem numerically.

In the present LSWF, we start from a weak form over a local sub-domain Ω_s , and use the MLS approximation to develop a true meshless method, where the local sub-domain Ω_s is located entirely inside the global domain Ω . The local sub-domain Ω_s is conveniently taken to be a sphere (in 3-D, or a circle in 2-D) centered at a point \mathbf{x} in question. A generalized local weak form of the differential equation (18) and the boundary conditions (19), over a local sub-domain Ω_s , can be written as:

$$\int_{\Omega_s} (\nabla^2 u - p)v \, d\Omega - \alpha \int_{\Gamma_{su}} (u - \bar{u})v \, d\Gamma = 0 \quad (20)$$

where u is the trial function, v is the test function, and Γ_{su} is a part of the boundary $\partial\Omega_s$ of Ω_s , over which the essential boundary conditions are specified. In general, $\partial\Omega_s = \Gamma_s \cup L_s$, with Γ_s being a part of the local boundary located on the global boundary and L_s being the other part of the local boundary over which no boundary condition is specified, i.e., $\Gamma_s = \partial\Omega_s \cup \Gamma$ and $L_s = \partial\Omega_s - \Gamma_s$ (see Fig. 3). If the sub-domain Ω_s is located entirely within the global

domain Ω , and there is no intersection between the local boundary $\partial\Omega_s$ and the global boundary Γ , the boundary integral over Γ_{su} vanishes. In Eq. (20), a penalty parameter $\alpha \gg 1$ is used to impose the essential boundary conditions, as the MLS approximation will be used to approximate the trial function, and it is not easy to directly impose the essential boundary conditions, a priori, in the MLS approximation.

Using $(\nabla^2 u)v = u_{,ii}v = (u_{,i}v)_{,i} - u_{,i}v_{,i}$, and the divergence theorem, yields the following expression:

$$\begin{aligned} & \int_{\partial\Omega_s} u_{,i}n_i v \, d\Gamma - \int_{\Omega_s} (u_{,i}v)_{,i} + pv \, d\Omega \\ & - \alpha \int_{\Gamma_{su}} (u - \bar{u})v \, d\Gamma = 0 \end{aligned} \quad (21)$$

in which $\partial\Omega_s$ is the boundary of the sub-domain Ω_s and n is the outward unit normal to the boundary $\partial\Omega_s$.

It should be noted that Eq. (21) holds irrespective of the size and shape of $\partial\Omega_s$. This is an important observation which forms the basis for the following development. We now deliberately choose a simple regular shape for Ω_s and thus for $\partial\Omega_s$. The most regular shape of a sub-domain should be an n -dimensional sphere for a boundary value problem defined on an n -dimensional space. Thus, an n -dimensional sphere (or a part of an n -dimensional sphere for a boundary node), is chosen in our development (see Fig. 3).

In the following development, the Petrov-Galerkin method is used. Unlike in the conventional Galerkin method in which the trial and test functions are chosen from the same space, the Petrov-Galerkin method uses the trial functions and the test functions from different spaces. In particular, the test functions need not vanish on the boundary where the essential boundary conditions are specified.

Imposing the natural boundary condition, $q = \bar{q}$, and noticing that $u_{,i}n_i = \partial u / \partial n \equiv q$ in Eq. (21), we obtain:

$$\begin{aligned} & \int_{L_s} qv \, d\Gamma + \int_{\Gamma_{su}} qv \, d\Gamma + \int_{\Gamma_{sq}} \bar{q}v \, d\Gamma - \int_{\Omega_s} (u_{,i}v)_{,i} + pv \, d\Omega \\ & - \alpha \int_{\Gamma_{su}} (u - \bar{u})v \, d\Gamma = 0 \end{aligned} \quad (22)$$

in which Γ_{sq} is a part of $\partial\Omega_s$, over which the natural boundary condition, $q = \bar{q}$, is specified. For a sub-domain located entirely within the global domain, there is no intersection between $\partial\Omega_s$ and Γ , $L_s = \partial\Omega_s$ and the integrals over Γ_{su} and Γ_{sq} vanish.

In order to simplify the above equation, we deliberately select a test function v such that it vanishes over L_s , the circle (for an internal node) or the circular arc (for a node on the global boundary Γ). This can be easily accomplished by using the weight function in the MLS approximation as also the test function, with the radius r_i of the support of the weight function being replaced by the radius r_0 of the local domain Ω_s , such that the test function vanishes on a circle of radius r_0 . Using this test function and rearranging Eq. (22), we obtain the following local symmetric weak form (LSWF):

$$\begin{aligned} & \int_{\Omega_s} u_{,i}v_{,i} \, d\Omega + \alpha \int_{\Gamma_{su}} uv \, d\Gamma - \int_{\Gamma_{su}} qv \, d\Gamma \\ & = \int_{\Gamma_{sq}} \bar{q}v \, d\Gamma + \alpha \int_{\Gamma_{su}} \bar{u}v \, d\Gamma - \int_{\Omega_s} pv \, d\Omega . \end{aligned} \quad (23)$$

With Eq. (23) for any point \mathbf{x} , the problem becomes one as if we are dealing with a localized boundary value problem over an n -dimensional sphere Ω_s . The radius of the sphere will affect the solution. In the present formulation, the equilibrium equation and the boundary conditions are satisfied, a posteriori, in all local sub-domains and on their Γ_s , respectively. Theoretically, as long as the union of all local domains covers the global domain, i.e., $\cup\Omega_s \supset \Omega$, the equilibrium equation and the boundary conditions will be satisfied, a posteriori, in the global domain Ω and on its boundary Γ , respectively. However, from our computation, the present formulation yields a very satisfactory result even when the union of all local domains does not cover the global domain.

4

Discretization and numerical implementation

As a known test function is used in the LSWF, the use of the LSWF for one point (and hence for one local domain) will yield only one linear equation involving $\hat{\mathbf{u}}$. Note that the trial function u within the sub-domain Ω_s , in the MLS approximation, is determined by the fictitious nodal values \hat{u}_i , within the ‘‘domain of definition’’ for all points \mathbf{x} falling within Ω_s . The LSWF, Eq. (23), gives one algebraic equation relating all these \hat{u}_i . Thus, one obtains as many equations as the number of nodes. Therefore, we need as many local domains Ω_s as the number of nodes in the global domain to obtain as many equations as the number of unknowns. In the present implementation, the local domain is chosen as a circle, centered at a node \mathbf{x}_i .

To obtain the discrete equations from the LSWF (23), the MLS approximation (11) is used to approximate the test function u . Substitution of Eq. (11) into the LSWF (23) for all nodes leads to the following discretized system of linear equations:

$$\mathbf{K} \cdot \hat{\mathbf{u}} = \mathbf{f} \quad (24)$$

where, the entries of the ‘‘stiffness’’ matrix \mathbf{K} and the ‘‘load’’ vector are defined by

$$\begin{aligned} K_{ij} &= \int_{\Omega_s} \phi_{j,k}(\mathbf{x})v_{,k}(\mathbf{x}, \mathbf{x}_i) \, d\Omega + \alpha \int_{\Gamma_{su}} \phi_j(\mathbf{x})v(\mathbf{x}, \mathbf{x}_i) \, d\Gamma \\ & - \int_{\Gamma_{sq}} \phi_{j,n}(\mathbf{x})v(\mathbf{x}, \mathbf{x}_i) \, d\Gamma \end{aligned} \quad (25a)$$

and

$$\begin{aligned} f_i &= \int_{\Gamma_{sq}} \bar{q}(\mathbf{x})v(\mathbf{x}, \mathbf{x}_i) \, d\Gamma + \alpha \int_{\Gamma_{su}} \bar{u}(\mathbf{x})v(\mathbf{x}, \mathbf{x}_i) \, d\Gamma \\ & - \int_{\Omega_s} p(\mathbf{x})v(\mathbf{x}, \mathbf{x}_i) \, d\Omega \end{aligned} \quad (25b)$$

in which ϕ_j is the shape function from the MLS approximation, and $(\)_{,n} = \partial(\) / \partial n$.

It can be easily seen that the system stiffness matrix in the present method is banded but unsymmetric. The locations of the non-zero entries in the system “stiffness” matrix depend upon all the nodes located within the domain of influence of the node in question, as shown in Fig. 3.

It should be noted that, in the present implementation, the test function v is selected to be the same as the weight function w_i in the MLS approximation used to approximate the trial function u . Fig. 4 shows the similarity between the test function in the LSWF, and the weight function in the MLS approximation.

The implementation of the present method can be carried out according to the following routine:

1. Choose a finite number of nodes in the domain Ω and on the boundary Γ of the given physical domain; decide the basis functions and weight functions such that the MLS approximation is well defined.
2. Determine the local sub-domain Ω_s and its corresponding local boundary $\partial\Omega_s$ for each node (see Fig. 3).
3. Loop over all nodes located inside the global domain and at the global boundary Γ

- Determine Gaussian quadrature points \mathbf{x}_Q in Ω_s and on $\partial\Omega_s$.
- Loop over quadrature points \mathbf{x}_Q in the sub-domain Ω_s and on the local boundary $\partial\Omega_s$
 - (a) determine the nodes \mathbf{x}_i located in the domain of definition of the MLS approximation for the trial function at point \mathbf{x}_Q , i.e., those nodes with $w_i(\mathbf{x}_Q) > 0$;
 - (b) for those nodes in the domain of definition of the MLS approximation of trial function at point \mathbf{x}_Q ; calculate $\phi_i(\mathbf{x}_Q)$ and the derivatives $\phi_{i,j}(\mathbf{x}_Q)$;
 - (c) evaluate numerical integrals in Eqs. (25a) and (25b);
 - (e) assemble contributions to the linear system for all nodes in K ; \mathbf{f} ;
 - (f) end if

- End quadrature point loop

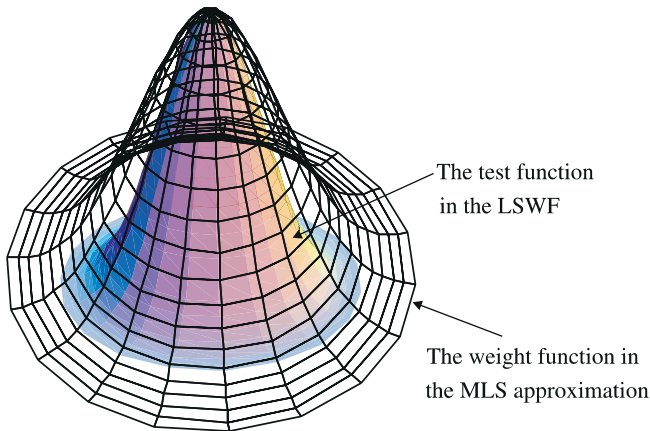


Fig. 4. The test function in the weak form and the weight function in the MLS approximation

4. End node loop.
5. Solve the linear system for the fictitious nodal values \hat{u} .
6. Calculate the value of the unknown variable and its derivatives by using Eq. (28) at those sample points under consideration.

From the above implementation, we can easily see that the present method is a truly meshless method, as absolutely no domain and boundary elements are needed, either for interpolation purposes or for integration purposes. The domain and boundary integrals in the present method can be easily evaluated over the regularly-shaped sub-domains (spheres in 3-D or circles in 2-D) and their boundaries.

5 Numerical examples

In this section, some numerical results are presented to illustrate the implementation and convergence of the present LSWF approach. For the purpose of error estimation and convergence studies, the Sobolev norms $\| \cdot \|_k$ are calculated. In the following numerical examples, the Sobolev norms for $k = 0$ and $k = 1$ are considered for the present potential problem. These norms are defined as:

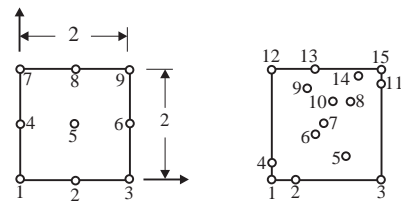
$$\|u\|_0 = \left(\int_{\Omega} u^2 d\Omega \right)^{\frac{1}{2}} \tag{26a}$$

and

$$\|u\|_1 = \left(\int_{\Omega} u^2 + (|\nabla u|)^2 d\Omega \right)^{\frac{1}{2}} . \tag{26b}$$

The relative errors are defined as

$$r_k = \frac{\|u^{num} - u^{exact}\|_k}{\|u^{exact}\|_k}, \quad k = 0, 1 . \tag{27}$$



a Regular nodes

b Irregular nodes

Coordinates for patch (b)

Nodes	
2	0.3,0.0
4	0.0,0.2
5	1.2,0.4
6	0.8,0.9
7	0.9,1.0
8	1.4,1.2
9	0.5,1.3
10	1.1,1.2
11	2.0,1.8
13	0.8,2.0
14	1.6,1.9

Fig. 5a-c. Nodes for the patch test

5.1 Patch test

Consider the standard patch test in a domain of dimension 2×2 as shown in Fig. 5, and a Dirichlet problem with $p = 0$ in Eq. (18) (i.e., the Laplace equation). We consider a problem with the exact solution

$$u = x^1 + x^2 \tag{28}$$

where the potential boundary condition Eq. (19a) is prescribed on all boundaries according to Eq. (28). Satisfaction of the patch test requires that the value of u at any interior node be given by the same linear function (28); and that the derivatives of the computed solution be constant in the patch.

Since the exact solution is a linear function of x^1 and x^2 , a linear basis for the MLS approximation is able to represent this solution. Note that the shape functions and their derivatives from the MLS approximation are no longer piecewise polynomials, and the numerical integration scheme will not yield accurate values for the matrices

in the linear system (24). In this example, 9 Gauss points are used on each section of Γ_s , and 5×8 points are used in the local domain Ω_s for numerical quadratures.

The nodal arrangements of all patches are shown in Fig. 5. Both Gaussian and spline weight functions are tested. In all cases, $r_i = 4$ and $r_i/c_i = 4$ are used in the computation. In Fig. 5, the coordinates of node 5 for mesh c1, c2, c3, c4, c5 and c6 are (1.1, 1.1), (0.1, 0.1), (0.1, 1.8), (1.9, 1.8), (0.9, 0.9) and (0.3, 0.4) respectively.

The computational results show that the present meshless method based on the LSWF passes all the patch tests in Fig. 5 for both Gaussian and spline weight functions with the given source function $p = 0$.

5.2 Laplace equation

The second example solved here is the Laplace equation in the 2×2 domain shown in Fig. 5, with the exact solution, a cubic polynomial, as

$$u = -(x^1)^3 - (x^2)^3 + 3(x^1)^2x^2 + 3x^1(x^2)^2 \tag{29}$$

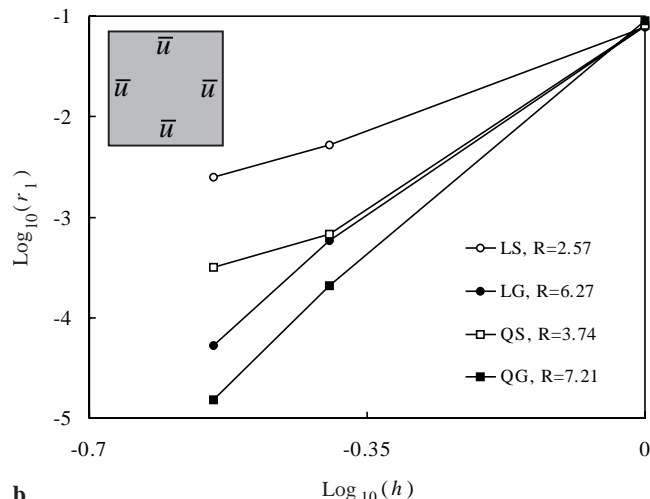
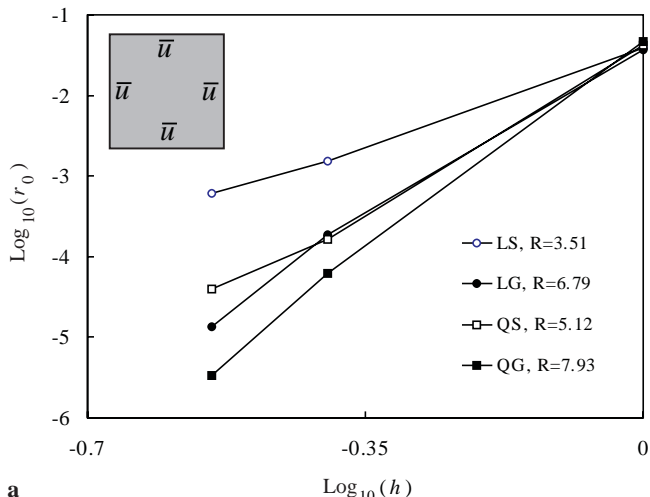


Fig. 6a,b. Relative errors and convergence rates for the Dirichlet problem of Laplace equation: **a** for norm $\|\cdot\|_0$, **b** for norm $\|\cdot\|_1$. In this figure and thereafter, R is the convergence rate; and “LS”, “LG”, “QS” and “QG” denote “Linear Spline”, “Linear Gaussian”, “Quadratic Spline” and “Quadratic Gaussian” respectively

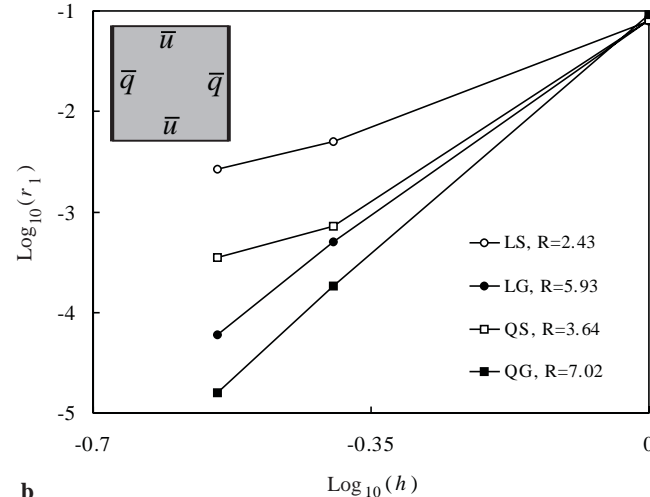
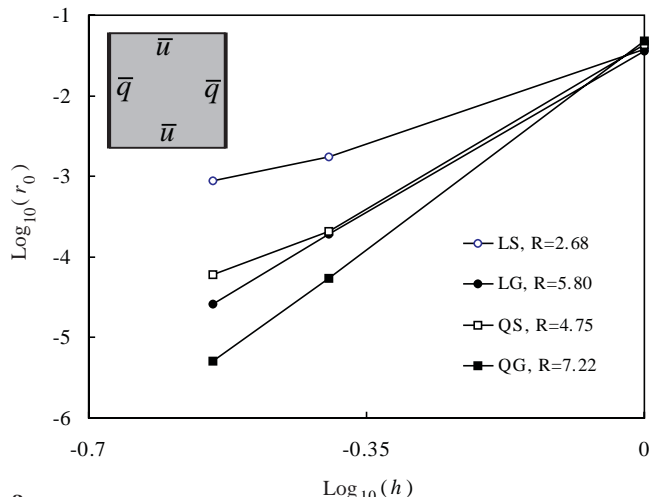


Fig. 7a,b. Relative errors and convergence rates for the mixed problem of Laplace equation: **a** for norm $\|\cdot\|_0$, **b** for norm $\|\cdot\|_1$

A Dirichlet problem is solved, for which the essential boundary condition is imposed on all sides, and a mixed problem, for which the essential boundary condition is imposed on top and bottom sides and the flux boundary condition is prescribed on left and right sides of the domain. The MLS approximation with both linear and quadratic bases as well as Gaussian and spline weight functions are employed in the computation. The size of support for both weight functions are taken to be $5h$ with h being the mesh size, and the parameter c_i for Gauss weight function is $r_i/4$.

Regular meshes of $9(3 \times 3)$, $36(6 \times 6)$ and $64(8 \times 8)$ nodes are used to study the convergence of the method. Also, 9 Gauss points are used on each section of Γ_s , and 5×8 points are used in the local domain Ω_s for numerical quadratures. The size (radius) of the local boundary for each node is chosen as h in the computation.

The convergence with mesh refinement of the present method is studied for this problem. The results of relative errors and convergence for norms $\|\cdot\|_0$ and $\|\cdot\|_1$ are shown in Fig. 6 for the Dirichlet problem and in Fig. 7 for the mixed problem, respectively.

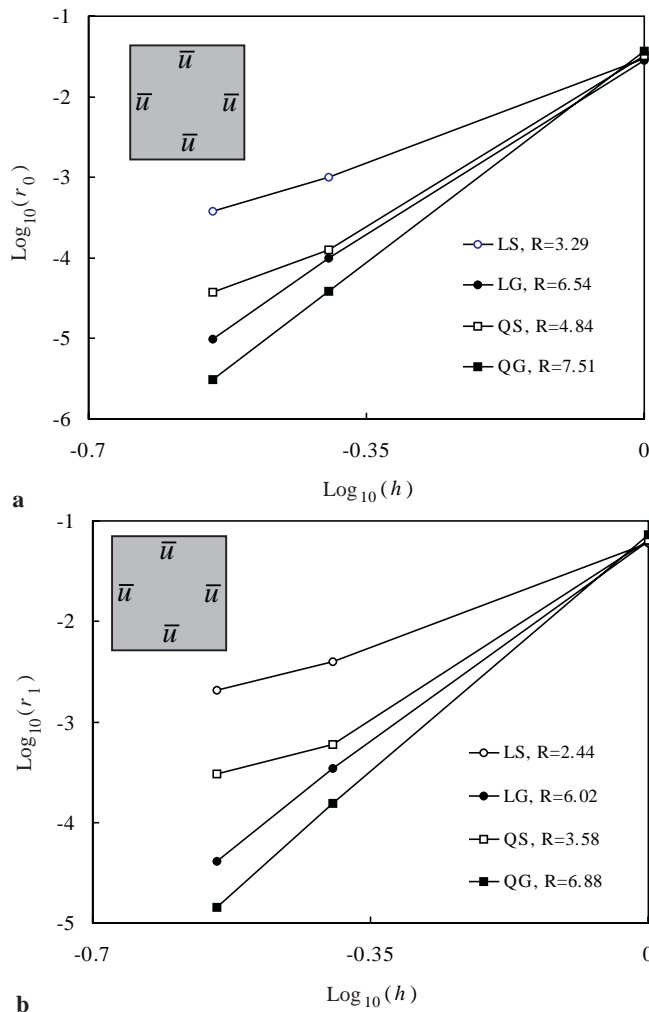


Fig. 8a,b. Relative errors and convergence rates for the Dirichlet problem of Poisson's equation: **a** for norm $\|\cdot\|_0$, **b** for norm $\|\cdot\|_1$

It can be seen that the present meshless method based upon the LSWF method has high rates of convergence for norms $\|\cdot\|_0$ and $\|\cdot\|_1$ and gives reasonably accurate results for the unknown variable and its derivatives.

5.3 Poisson's equation

The results from the present meshless LSWF formulation are also studied for the Poisson's equation with a given source function $p = x^1 + x^2$ in the same 2×2 domain, for which the exact solution is taken to be

$$u = -\frac{5}{6}[(x^1)^3 + (x^2)^3] + 3(x^1)^2x^2 + 3x^1(x^2)^2. \quad (30)$$

The boundary conditions, the size of local boundary, the parameters c_i and r_i in the MLS approximation as well as the nodal arrangement are the same as those used in the last example. Also, the MLS approximations with both linear and quadratic bases as well as Gaussian and spline weight functions are tested in the computation.

The convergence with mesh refinement of the present method is studied for this problem. The results of relative

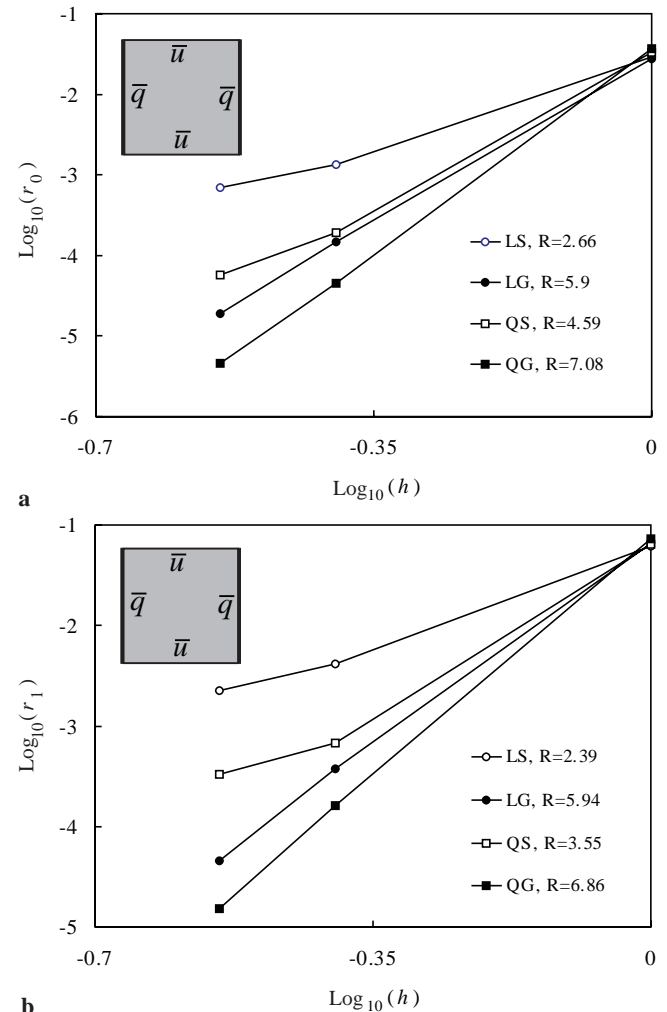


Fig. 9a,b. Relative errors and convergence rates for the mixed problem of Poisson's equation: **a** for norm $\|\cdot\|_0$, **b** for norm $\|\cdot\|_1$

errors and convergence for the $\|\cdot\|_0$ and $\|\cdot\|_1$ norms are shown in Fig. 8 for the Dirichlet problem and in Fig. 9 for the mixed problem, respectively. These figures show that the present meshless method works quite well for the Poisson's equation.

5.4 Potential flow

Consider the problem of a potential flow around a cylinder of radius a in an infinite domain, shown in Fig. 10. u represents the stream function.

Due to symmetry, here only a part, $0 \leq x^1 \leq 4$ and $0 \leq x^2 \leq 2$, of the upper left quadrant of the field is modeled as shown in Fig. 10. The exact solution for this problem is given by

$$u = x^2 \left[1 - \frac{x^1}{(x^2)^2 + (x^1 - L)^2} \right]. \quad (31)$$

Fig. 10 shows the prescribed u and $\partial u / \partial n$ values along all boundaries. The essential boundary condition on the left and top edges is imposed according to the exact solution (31).

The initial mesh of 26 nodes is considered as shown in Fig. 11(a). Subsequently, the number of nodes is increased to 47 in Fig. 11(b) and 74 in Fig. 11(c) to study the convergence with mesh refinement of the present meshless method.

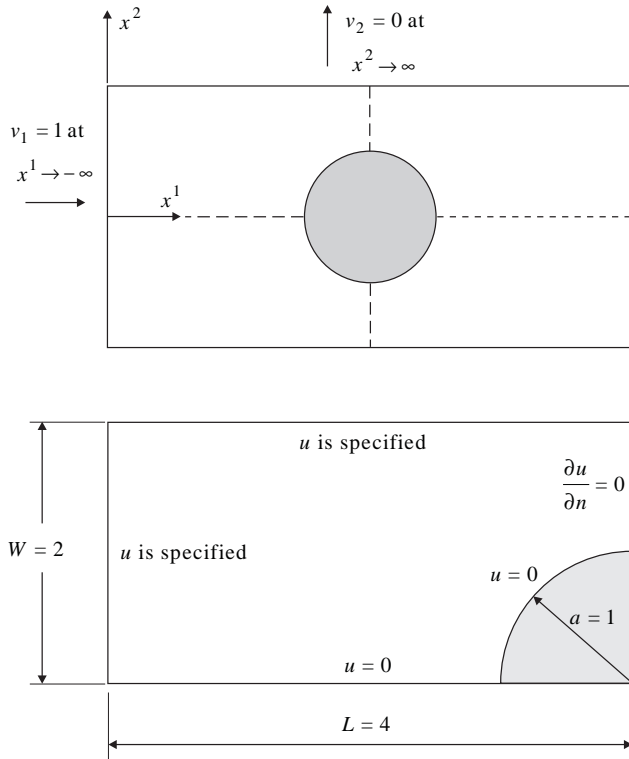
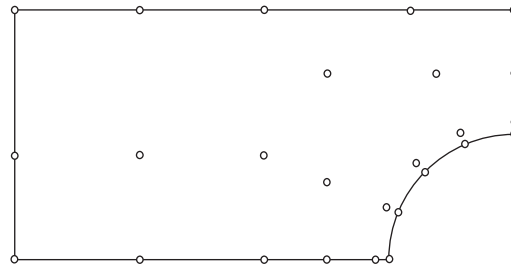
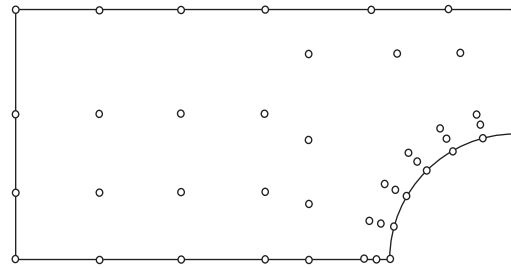


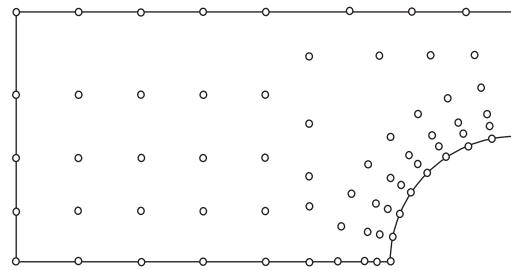
Fig. 10. Flow around a cylinder in an infinite field and the model with boundary conditions



a 26 nodes



b 47 nodes



c 74 nodes

Fig. 11a-c. Flow around a cylinder: nodal arrangement

Both linear and quadratic bases as well as Gaussian and spline weight functions are considered. We use $c_i = l_i$ and $r_i = 4c_i$ in the calculation, where l_i is defined as:

$$l_i = 2 \max_{j \in S_j} \|\mathbf{x}_j - \mathbf{x}_i\| \quad (32)$$

where S_j is the minimum set of neighboring nodes of \mathbf{x}_i which construct a polygon surrounding \mathbf{x}_i .

The convergence for the Sobolev norms $\|\cdot\|_0$ and $\|\cdot\|_1$ is shown in Fig. 12. The mesh size h in this problem is defined as the average mesh sizes on the bottom edge.

The stream lines from the exact solution and from the numerical solution of the present meshless formulation with a linear basis and Gaussian weight functions for the cases of 26 and 47 nodes are also shown in Fig. 13. It can be seen that the stream lines are well approximated by the present method with 47 nodes as compared to the closed form solution.

From these examples, it can be seen that the quadratic basis yields somewhat of a better result than the linear basis while both bases possess high accuracy. Also, the Gauss weight function works better than the spline weight function. We should keep in mind that the appropriate parameters c_i in Eq. (16) need to be determined for all nodes for the Gauss weight function. The values of these parameters

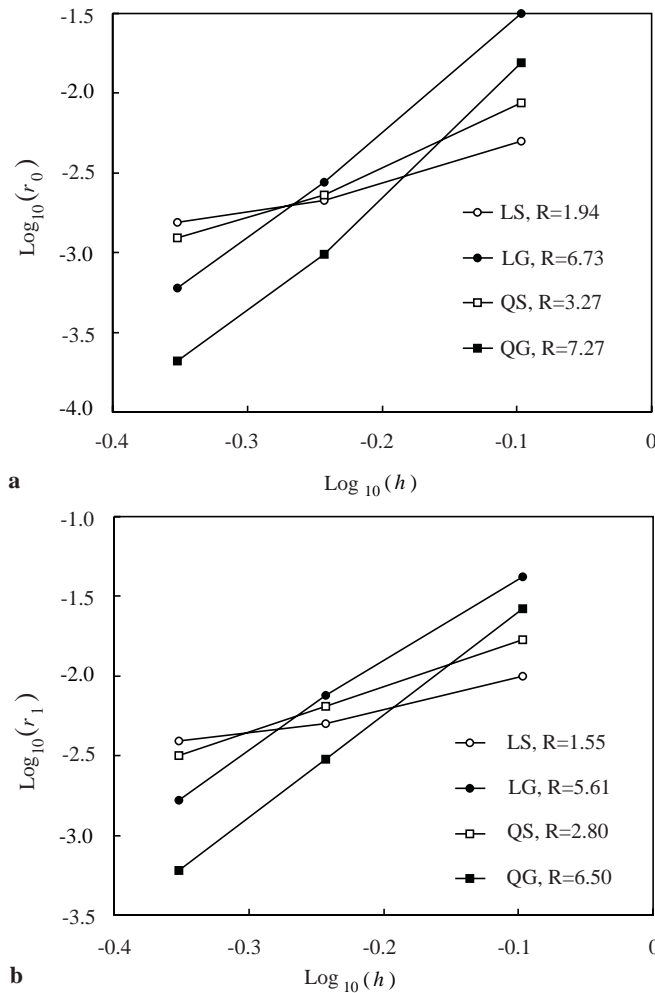


Fig. 12a,b. Relative errors and convergence rates for the potential flow problem: **a** for norm $\|\cdot\|_0$, **b** for norm $\|\cdot\|_1$

will effect the numerical results considerably. With inappropriate c_i used in the Gaussian weight function, the results may become very unsatisfactory. The optimal choice of these parameters is still an open research topic.

6 Conclusions and discussions

A novel and truly meshless method, based on the presently proposed local symmetric weak form is developed in the present paper. As is the case with other meshless methods based on a global Galerkin method, the present method also possesses the following advantages over the finite element method.

- The present method is considerably more accurate for computing the values of the unknown variable and its derivatives than the finite element method.
- No smoothing technique is required to compute the derivatives, as the original result is smooth enough.
- No element connectivity is needed; and only randomly distributed nodal points are constructed.

Convergence studies in the numerical examples show that the present method possesses an excellent rate of convergence for both the unknown variable and its deriva-

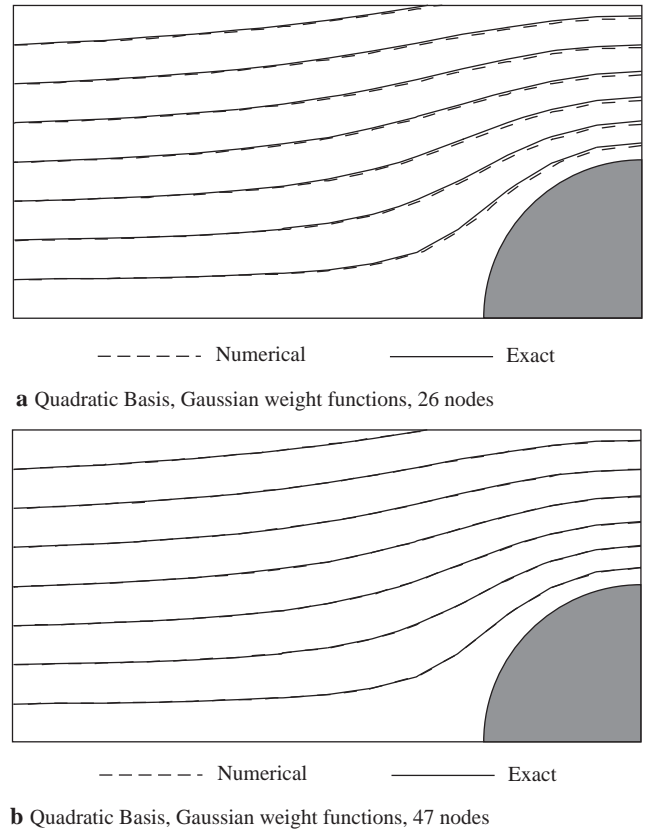


Fig. 13. The stream lines of the flow problem

tives. Only a simple numerical manipulation is needed for calculating the derivatives of the unknown function as the original approximated trial solution is smooth enough to yield reasonably accurate results for derivatives. The numerical results show that using both linear and quadratic bases as well as spline and Gaussian weight functions in the approximation function can give quite accurate numerical results.

Compared with the other meshless techniques, discussed in literature, based on a global Galerkin formulation (for instance, the EFG method), the present approach is found to have the following advantages.

- Absolutely no elements are needed in the present formulation, either for interpolation purposes or for integration purposes, while shadow elements are required in the EFG method to evaluate volume integrals.
- No special integration scheme is needed to evaluate the volume and boundary integrals. The integrals in the present method are evaluated only over regularly-shaped sub-domains and their boundaries. The local boundary in general is the surface of a “unit sphere” centered at the node in question. This flexibility in choosing the size and the shape of the local sub-domain will lead to a more convenient formulation in dealing with the non-linear problems.

Besides, the current formulation possesses flexibility in adapting the density of the nodal points at any place of the problem domain such that the resolution and fidelity of the solution can be improved easily. This is especially

useful in developing intelligent, adaptive algorithms based on error indicators, for engineering applications.

The present method possesses a tremendous potential for solving nonlinear problems and/or problems with discontinuities. Further results in using the current approach in some solid mechanics problems will be presented in a series of forthcoming papers.

In view of the local weak form, and the nature of the trial and test functions, used in this paper, we label the approach described in this paper for future reference as, “Meshless Local Petrov-Galerkin (MLPG) method”.

References

Belytschko T, Lu YY, Gu L (1994) Element-free Galerkin methods. *Int. J. Numer. Methods Eng.* 37:229–256
Liu WK, Chen Y, Chang CT, Belytschko T (1996) Advances in multiple scale kernel particle methods. *Comput. Mech.* 18:73–111

Mukherjee YX, Mukherjee S (1997) On boundary conditions in the element-free Galerkin method. *Comput. Mech.* 19:264–270
Nayroles B, Touzot G, Villon P (1992) Generalizing the finite element method: diffuse approximation and diffuse elements. *Comput. Mech.* 10:307–318

Organ D, Fleming M, Terry T, Belytschko T (1996) Continuous meshless approximations for nonconvex bodies by diffraction and transparency. *Comput. Mech.* 18: 225–235

Zhu T, Atluri SN (1998) A modified collocation & a penalty formulation for enforcing the essential boundary conditions in the element free Galerkin method. *Comput. Mech.* 21: 211–222

Zhu T, Zhang J-D, Atluri SN (1998a) A local boundary integral equation (LBIE) method in computational mechanics, and a meshless discretization approach. *Comput. Mech.* 21: 223–235

Zhu T-L, Zhang J-D, Atluri SN (1998b) A meshless local boundary integral equation (LBIE) method for solving nonlinear problems. *Comput. Mech.* In press